

Synthesis and characterization of triflic acid-functionalized mesoporous Zr-TMS catalysts: heterogenization of $\text{CF}_3\text{SO}_3\text{H}$ over Zr-TMS and its catalytic activity

M. Chidambaram,^a D. Curulla-Ferre,^b A.P. Singh,^{a,*} and B.G. Anderson^b

^a Catalysis Division, National Chemical Laboratory, Pune 411008, India

^b Schuit Institute of Catalysis, Eindhoven University of Technology, PO Box 513, 5600 MB Eindhoven, The Netherlands

Received 1 April 2003; revised 18 June 2003; accepted 18 June 2003

Abstract

Triflic acid-functionalized Zr-TMS (zirconium oxide with a mesostructured framework; TMS, transition metal oxide mesoporous molecular sieves) catalysts have been synthesized by functionalizing triflic acid onto the walls of Zr-TMS via post synthesis method. The synthesized materials were characterized by powder XRD, N_2 -sorption, FT-IR spectroscopy, elemental analysis, solid-state ^{13}C CP and DD/MAS NMR spectroscopy, FT-Raman analysis, NH_3 -TPD, SEM, TEM, TG-DTA, and DTG techniques. All these results revealed that an ordered Zr-TMS material was synthesized and triflic acid was anchored on the walls of the Zr-TMS. Typical XRD patterns of the Zr-TMS and functionalized Zr-TMS (f-Zr-TMS) showed ordered structures. Synthesized materials showed type IV isotherms. The chemical shift observed (≈ 119 ppm) and ^{13}C – ^{19}F coupling ($J_{\text{C-F}} \approx 310$ Hz) by ^{13}C DD/MAS NMR showed that the triflic acid was intact on the catalyst framework. According to Raman spectral analysis, triflate was adsorbed on the zirconia surface at all loadings as a tridentate ligand through three equivalent S–O bonds (local C_{3v} symmetry). Ammonia TPD measurements revealed an increase in number of acid sites with an increase in loading of triflic acid. Functionalized amorphous $\equiv\text{Zr-O-SO}_2\text{-CF}_3$ catalysts were also synthesized by an in situ method and $\text{SO}_4^{2-}/\text{ZrO}_2$ was obtained for comparison. The catalytic activity of the materials was tested in the acetalization of ethylacetoacetate and in the benzylation of biphenyl in a batch reactor at 100 and 150 °C, respectively. Recycling was performed in the acetalization of ethylacetoacetate using f-Zr-TMS-30 three times and no major deactivation of the catalyst was observed.

© 2003 Elsevier Inc. All rights reserved.

Keywords: f-Zr-TMS; Triflic acid; Functionalization; Acetalization of ethylacetoacetate; Benzylation of biphenyl

1. Introduction

Synthesis of highly acidic inorganic materials by heterogenization of homogeneous systems is currently the subject of a great deal of research in green chemistry that aims to facilitate the recovery of the catalyst and to minimize the pollution. Many acidic catalysts have been developed using silica, alumina, metal oxides, and microporous zeolites as supports [1–5]. However, there are still many problems because of limited acidity and diffusion. Soon after the discovery of the MCM-41 materials, it was demonstrated that it is also possible to synthesize non-silica-based mesostructured materials. Niobium-, hafnium-, or cerium-based materials are now frequently cited [6–8]. However, as noted in a recent review

by Sayari and Liu [9], although a large number of elements are able to form such materials, only few of these exhibit ordered porous structures.

Transition metal oxides are widely used as industrial catalysts and as catalyst supports. Unfortunately they usually have poorly defined pore structures. The synthesis of mesoporous silica partially substituted by titanium and zirconium has been attempted to circumvent the difficulty of preparing stable mesoporous titania and zirconia. Zirconium oxide is of particular interest because it contains both acidic and basic surface sites. These are critical for some reactions that need bifunctional (amphoteric) catalysts. The search for zirconium oxide as supports for various catalysts has received keen interest in the past decade. In recent years $\text{SO}_4^{2-}/\text{ZrO}_2$ has attracted attention as it catalyzes various industrially important reactions such as isomerization, condensation, and Friedel–Crafts acylation reactions [10]. However, its nonuni-

* Corresponding author.

E-mail address: apsingh@cata.ncl.res.in (A.P. Singh).

form pore size, low porosity, and small surface area limit its potential application for catalyzing reactions of bulky molecules. Despite these limitations zirconia has a high melting point, low thermal conductivity, high corrosion resistance, and amphoteric behavior, all of which can be useful properties for a support material. The possibility of obtaining such material with a mesoporous texture has made this oxide even more interesting [11].

The recent discoveries of ordered, high surface area, porous zirconia in the presence of cationic surfactants by Knowles and Hudson [12,13], mesoporous zirconia from anionic and neutral surfactants by Pacheco et al. [14], nanostructured mesoporous zirconia by Blin et al. [15], mesoporous sulfated zirconium dioxide by Huang et al. [16], surfactant-assisted synthesis of mesoporous zirconia by Larsen et al. [17], and aluminum-doped mesoporous zirconia by Zhao et al. [18] are attracting increased interest in the use of zirconia as a catalyst support. Great effort has been made to prepare mesoporous zirconium hydroxide with high surface area via a surfactant templating route.

“Triflic acid (trifluoromethanesulfonic acid, $\text{CF}_3\text{SO}_3\text{H}$) is known to be a ‘strong’ acid.” It is widely used in many organic reactions such as Koch carbonylations [19], Friedel–Crafts reactions [20], polymerizations [20], etc. [21,22]. However, the recovery of the triflic acid from the reaction mixture results in the formation of large amounts of waste, which is environmentally unacceptable. The desire to perform acid-catalyzed reactions over solids has resulted in new research in this area and supported triflic acid is now becoming available to replace homogeneous acid solutions [23–25].

Trifluoromethanesulfonic acid and its conjugate base have extremely high thermal stability and resistance to both reductive and oxidative cleavage. They do not provide a source of fluoride ions even in the presence of strong nucleophiles. In addition, the use of triflates or triflic acid as homogeneous acid catalysts has received attention because of the electron-withdrawing effect exerted by the trifluoromethanesulfonyl group. Recently, a silica-supported polytrifluoromethanesulfosiloxane solid superacid [26], a silica-embedded triflate [27], and metal-triflate [28] were reported to be heterogeneous catalysts for reactions of bulkier molecules. Hence, we thought that the immobilization of triflic acid over Zr-TMS would develop a novel class of heterogeneous solid acid catalysts with enhanced acidity. Moreover, the use of a heterogeneous $\text{CF}_3\text{SO}_3\text{H}$ system would offer ease of catalyst recovery and reuse, and minimize the production of waste currently formed during triflic acid recovery.

In this paper, we disclose the first preparation of triflic acid functionalized Zr-TMS (f-Zr-TMS, $\text{Zr-TMS-O-SO}_2\text{-CF}_3$, mesoporous $\equiv\text{Zr-O-SO}_2\text{-CF}_3$) materials using Zr-TMS as solid support and triflic acid as an acidic component (added by post synthesis). Sol-gel method was employed for the synthesis of Zr-TMS. The environment of the triflic acid on the walls of Zr-TMS was deter-

mined by different techniques. Since the catalysts are highly acidic, acetalization of ethylacetoacetate (EAA) to ethyl 3,3-ethylenedioxybutyrate (fructose) and benzylation of biphenyl (BP) to 4-phenylbenzophenone (4-PBP) were carried out to check the catalytic activity of the synthesized catalysts. Both reactions were also carried out by using functionalized amorphous $\equiv\text{Zr-O-SO}_2\text{-CF}_3$ catalysts, Zr-TMS, $\text{SO}_4^{2-}/\text{ZrO}_2$, and triflic acid for comparison. Fructose, an apple scent has been used as fragrance, in detergents, in pharmaceutical industries, as food and beverage additives, and also in cosmetics [29]. The 4-PBP is an important intermediate in the pharmaceutical industry to synthesize an antifungal agent (bifonazole) and as a photo-initiator [30,31].

2. Experimental

2.1. Materials

The syntheses of f-Zr-TMS catalysts were carried out using zirconium (IV) butoxide (80 wt% solution in 1-butanol, Aldrich, USA), a 25 wt% aqueous solution of tetramethylammonium hydroxide (TMAOH, Loba Chemie, India), a 25 wt% aqueous solution of *N*-cetyl-*N,N,N* trimethylammonium bromide (CTMABr, Loba Chemie, India), and trifluoromethanesulfonic acid ($\text{CF}_3\text{SO}_3\text{H}$, Lancaster, UK).

2.2. Synthesis of Zr-TMS

The synthesis of Zr-TMS was carried out using the following gel composition and procedure: 0.07 $\text{Zr}(\text{OC}_4\text{H}_9)_4$:1.4 BuOH:0.02 CTMABr:0.014 TMAOH:1.7 H_2O .

A mixture of zirconium (IV) butoxide (80 wt% solution in 1-butanol) and 1-butanol was stirred for 10 min. Then the required amount of water was added dropwise into this mixture under stirring to hydrolyze the zirconium (IV) butoxide to $\text{Zr}(\text{OH})_4$. The precipitated $\text{Zr}(\text{OH})_4$ mixture was added to an aqueous solution of CTMABr (25 wt% aq solution) and TMAOH (25 wt% aq solution) under continuous stirring. After further stirring for 2 h, the resulting synthesis gel (pH = 10.5–11.0) was transferred to a round bottom flask, sealed, and refluxed at 90 °C for 48 h under stirring. The solid product was recovered by filtration, washed with deionized water and acetone, and dried at 100 °C for 2 h. The surfactant was removed from the synthesized material by extraction with a mixture containing 100 g of ethanol and 2.5 g of HCl (36 wt%) per gram of the solid material [20,32] under reflux for 48 h. The Zr-TMS was washed with water and acetone and dried at 100 °C for 6 h.

2.3. Synthesis of f-Zr-TMS catalysts

The resulting solid mesoporous material, Zr-TMS, was functionalized with triflic acid by post synthesis procedure using the molar composition 0.07 Zr-TMS:0.7 dry toluene:0.03 $\text{CF}_3\text{SO}_3\text{H}$.



Scheme 1.

Triflic acid (0.03 mol) was added dropwise into the mixture of toluene and Zr-TMS at 90 °C under nitrogen atmosphere and further refluxed for 2 h. Then the mixture was cooled, filtered, washed with acetone, and dried at 100 °C for 6 h. Soxhlet extraction of the material (to remove the unreacted triflic acid) was carried out at 75 °C for 24 h using a mixture of dichloromethane (100 g) and diethyl ether (100 g) per gram of catalyst. The sample was then dried at 200 °C for 10 h. The synthesis of the catalyst is shown in Scheme 1. The syntheses of different loadings of triflic acid (5 to 25 wt%) on Zr-TMS were carried out by varying the molar ratios of zirconium (IV) butoxide, CTMABr, TMAOH, water, and CF₃SO₃H.

2.4. Synthesis of functionalized amorphous

$\equiv\text{Zr-O-SO}_2\text{-CF}_3$

Synthesis of functionalized amorphous $\equiv\text{Zr-O-SO}_2\text{-CF}_3$ catalysts was carried out via the following procedure. A mixture of zirconium (IV) butoxide (0.07 mol) and 1-butanol (1.4 mol) was placed in a three-necked 250-ml round-bottom flask equipped with a magnetic stirrer and a septum. The flask was held at 90 °C and stirred for 10 min. Then 0.28 mol of water was added dropwise into this mixture under stirring to hydrolyze the zirconium (IV) butoxide to Zr(OH)₄. Further, after 30 min of stirring, triflic acid (0.03 mol) was slowly added by syringe into the above mixture and stirring was continued for 2 h. The mixture was cooled, filtered, washed with deionized water and acetone, and then dried at 100 °C for 6 h. Soxhlet extraction was carried out for 24 h. Then the sample was dried at 200 °C for 10 h. The syntheses of different loadings of triflic acid over amorphous Zr(OH)₄ (5 to 25 wt%) were carried out by varying the molar ratios of zirconium (IV) butoxide, water, and CF₃SO₃H. The synthesized materials were white in color. Functionalized amorphous materials are designated as $\equiv\text{Zr-O-SO}_2\text{-CF}_3$ (A).

The SO₄²⁻/ZrO₂ was obtained from MEL Chemicals (Manchester, UK) and activated at 500 °C for 10 h in static air prior to the catalytic run.

2.5. Catalyst characterization

The synthesized materials were mainly characterized by powder X-ray diffraction (XRD) for phase purity and crystallinity, N₂ adsorption–desorption techniques for specific surface area, total pore volume and average pore diameter, Fourier transform infrared (FTIR) spectroscopy for functional group confirmation, elemental analysis for C and S to measure the triflic acid loading in the material, solid-state

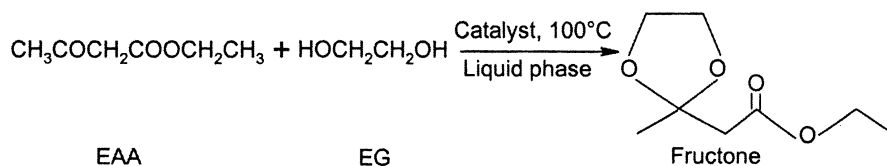
¹³C CP/MAS (cross-polarization/magic-angle spinning) and ¹³C DD/MAS (dipolar decoupled/magic angle spinning) NMR for the confirmation of functional group (–CF₃) in the catalyst, FT-Raman analysis for the binding mode of the triflate, temperature-programmed desorption (TPD) of NH₃ measurement for total acidity, scanning electron microscopy (SEM) for the particle size and morphology, transmission electron microscopy (TEM) to view the crystalline structure, and thermogravimetric-differential thermal analysis (TG-DTA and DTG) to study the decomposition and thermal stability of the catalysts.

The powder X-ray diffraction patterns of synthesized Zr-TMS, f-Zr-TMS, and $\equiv\text{Zr-O-SO}_2\text{-CF}_3$ (A) were recorded on a Rigaku D MAX III VC (Ni-filtered Cu-K_α radiation, λ = 1.5404 Å) between 1.5 and 60° (2θ) with a scan rate of 4°/min. The BET surface area, total pore volume, and average pore diameter were measured by N₂ adsorption–desorption method by NOVA 1200 (Quantachrome) at –196 °C. For this particular measurement, the samples were activated at 180 °C for 3 h under vacuum and then the adsorption–desorption was conducted by passing nitrogen onto the sample, which was kept under liquid nitrogen. The FT-IR spectra were obtained in a range of 400 to 4000 cm^{–1} on a Shimadzu FTIR 8201 PC using a diffuse reflectance scanning disk technique. Elemental analysis for C and S were done by an EA1108 elemental analyser (Carlo Erba Instruments).

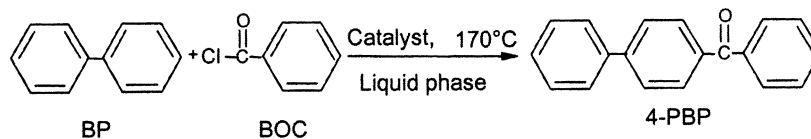
¹³C CP/MAS and ¹³C DD/MAS solid-state NMR studies were carried out on a Bruker DRX-500 NMR spectrometer. The resonance frequency was 125.757 MHz. The finely powdered sample f-Zr-TMS-30 was placed in 4.0-mm zirconia rotors and spun at 810 kHz. The CP/MAS spectrum was recorded under Hartmann-Hahn match conditions using a contact time of 1 m/s. A relaxation delay of 10 and 4 s was used for DD/MAS and CP/MAS spectra, respectively. The chemical shift was referred to an external adamantane CH₂ peak reference taken as 28.7 ppm with respect to TMS. The raw data obtained for DD/MAS (2000 scans) and CP/MAS (3000 scans) were processed with an exponential function of line broadening of 20 and 60 Hz, respectively, prior to Fourier transformation for sensitivity enhancement.

Powder samples (ca. 10 mg) were compressed into a small stainless-steel holder. Raman spectra of these samples were measured at room temperature, exposed to atmosphere, using a Bruker RFS/100S FT-Raman spectrometer. A Nd-YAG laser (1064 cm^{–1}; 50 mW) was used as an excitation source. Scattered radiation was collected at 180 °C and detected using an InGaAs detector. Spectra were recorded in the Stokes region between 2000 and 25 cm^{–1} at 4 cm^{–1} resolutions. One hundred scans were coadded. For comparison, the Raman spectrum of liquid triflic acid (Aldrich, synthesis grade; in a standard 4-mm NMR tube) was collected under similar conditions. Only 50 scans needed to be coadded.

Temperature-programmed desorption was carried out to determine the total acidity and strength of acid sites on the catalysts using ammonia as an adsorbate [33]. In a typi-



Scheme 2.



Scheme 3.

cal run, 1.0 g of activated sample was placed in a silica tubular reactor and heated at 200 °C under nitrogen flow of 50 ml/min for 6 h. The reactor was then cooled at 30 °C and adsorption conducted at that temperature by exposing the sample to ammonia (10 ml/min) for 30 min. Physically adsorbed ammonia was removed by purging the sample with a nitrogen stream flowing at 50 ml/min for 15 h at 30 °C. The acid strength distribution was obtained by raising the catalyst temperature (10 K/min) from 30 to 300 °C in a number of steps with the flow of nitrogen (50 ml/min). The NH₃ evolved was trapped in the HCl solution and titrated with a standard NaOH solution.

The SEM micrographs of Zr-TMS and f-Zr-TMS-30 materials were taken by JEOL-JSM-5200 scanning microscopy. TEM was performed on a JEOL JEM-1200EX instrument with 100 kV of acceleration voltage to probe the mesoporosity of the materials. The TG-DTA and DTG analysis of the Zr-TMS and f-Zr-TMS-30 catalysts were carried out with a Mettler Toledo 851^e equipment using an alumina pan under a nitrogen (80 ml/min) atmosphere from ambient to 1000 °C with an increasing rate of 20 °C/min.

2.6. Catalytic activity

The catalytic activity of all f-Zr-TMS was examined in the acetalization of ethylacetoacetate with ethylene glycol (EG) using toluene as a solvent (Scheme 2) and benzylation of biphenyl with benzoyl chloride (BOC) using nitrobenzene as a solvent (Scheme 3). The reactions were carried out in a batch reactor equipped with two-necked 50-ml round-bottom flask with septum, an oil bath, and condenser. AR grade chemicals were used without further purification. In a typical run, EAA and EG were added in a required molar ratio to the activated catalyst (0.1 g). In another run, BP and BOC were added to the activated catalyst (0.5 g) in the required molar ratio. The reaction mixtures were magnetically stirred and heated to the required temperature at atmospheric pressure. The products were analyzed in a gas chromatograph (HP 6890) equipped with a flame ionization detector (FID) and a capillary column (5- μm -thick cross-linked methyl silicone gum, 0.2 \times 50 m). The products were

also identified by GC-MS (Shimadzu 2000 A) analysis and confirmed by ¹H and ¹³C NMR spectra (Bruker AC-200).

Recycling of the catalyst was done during the acetalization reaction by using f-Zr-TMS-30. After workup of the reaction, the catalyst was separated by filtration, washed with acetone, and dried at 200 °C for 10 h in the presence of air. The recovered catalyst after each cycle was characterized for its crystallinity by XRD and its chemical composition by elemental analysis.

3. Results and discussion

3.1. Powder X-ray diffraction study

The powder X-ray diffraction (XRD) patterns of all the synthesized catalysts are shown in Fig. 1. The template-extracted Zr-TMS (Fig. 1A, Zr-TMS) and f-Zr-TMS (Fig. 1A, 5–30 wt%) catalysts exhibited a single, broad reflection at low 2θ (2.5–4.0°). This reflection corresponds to the XRD pattern of ordered mesoporous ZrO₂ [11,13–18] and Si-Zr mesoporous materials [34]. However, in these studies no higher order reflections were observed. The presence of these in our spectra may indicate that the pore walls are rather amorphous or that there is a lack of correspondence between the structures of adjacent pores. Other reflections were observed at about 31° (broad) and at about 50° (small) in all the samples. They are attributed to the tetragonal, monoclinic, and cubic phases of ZrO₂. They are readily formed after calcination of the sample at higher temperature [15]. The broad reflection at $2\theta = 31^\circ$ may also be partially due to the presence of amorphous materials as was reported in siliceous MCM-41 [35]. The crystallinity of the triflic acid containing Zr-TMS materials decreased as the triflic acid loading increased. Moreover, low intensity and the absence of higher order reflections show that the order and mesostructure were entirely different from that measured for the mesoporous silica [11]. $\equiv\text{Zr-O-SO}_2\text{-CF}_3$ (A) catalysts (Fig. 1B, 5–30 wt%) were indeed purely amorphous showing low intensity reflections at about 5, 31, and 50° (2θ).

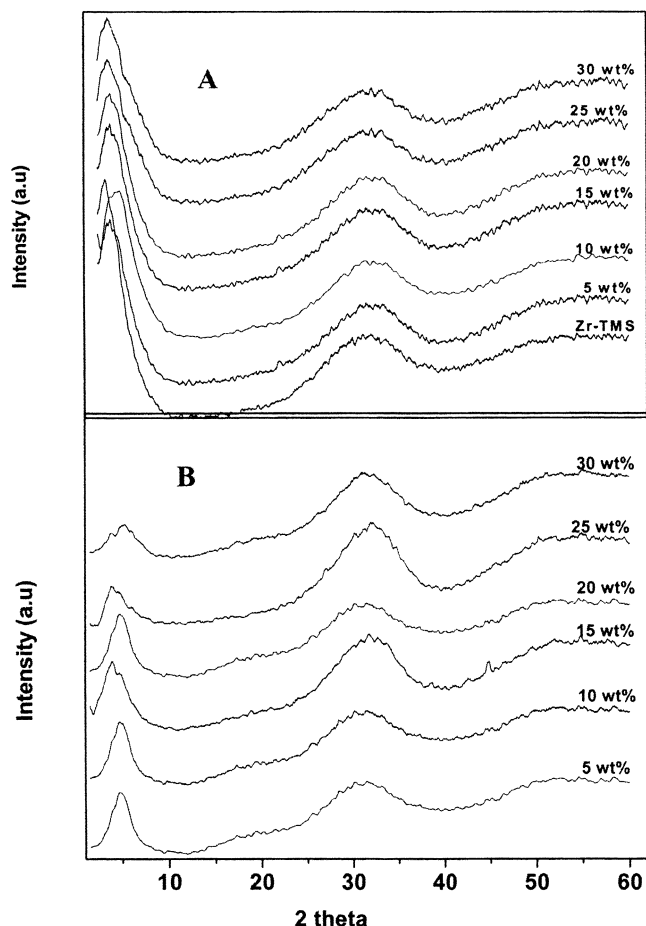


Fig. 1. XRD patterns of (A) Zr-TMS and f-Zr-TMS (5–30 wt%) and (B) $\equiv\text{Zr-O-SO}_2\text{-CF}_3$ (A) (5–30 wt%).

3.2. Nitrogen adsorption–desorption study

The incorporation or anchoring of any medium (acid or base) or metal in the framework positions and/or into the walls of the supporting medium leads to a progressive decrease in surface area [27,34,36]. The BET surface area of the Zr-TMS, f-Zr-TMS, $\equiv\text{Zr-O-SO}_2\text{-CF}_3$ (A), and $\text{SO}_4^{2-}/\text{ZrO}_2$ are given in Table 1. The surface area for the Zr-TMS was $371 \text{ m}^2 \text{ g}^{-1}$, which is comparable to that measured previously for a Zr-TMS synthesized using a surfactant with C₁₆ carbon chain [11,13]. Surface area gradually decreased with increasing triflic acid loading. The surface area decreased to $284 \text{ m}^2 \text{ g}^{-1}$ for the maximum loading of triflic acid (30 wt%) over Zr-TMS. In the same way, the surface area of amorphous Zr(OH)_4 was $80 \text{ m}^2 \text{ g}^{-1}$ and decreased to $52 \text{ m}^2 \text{ g}^{-1}$ for $\equiv\text{Zr-O-SO}_2\text{-CF}_3$ (A), 30. The surface area of $\text{SO}_4^{2-}/\text{ZrO}_2$ was found to be $101 \text{ m}^2 \text{ g}^{-1}$.

Zr-TMS and f-Zr-TMS-30 were analyzed by detailed N₂ sorption studies. The BET surface area, average pore diameter, and total pore volume of Zr-TMS and f-Zr-TMS-30 were $371 \text{ m}^2 \text{ g}^{-1}$, 44.3 \AA , $0.31 \text{ cm}^3 \text{ g}^{-1}$, and $284 \text{ m}^2 \text{ g}^{-1}$, 34.0 \AA , $0.25 \text{ cm}^3 \text{ g}^{-1}$, respectively (Table 1). The decrease in surface area, pore diameter, and pore volume of f-Zr-TMS-30 may be attributed to the functionalization of Zr-TMS by

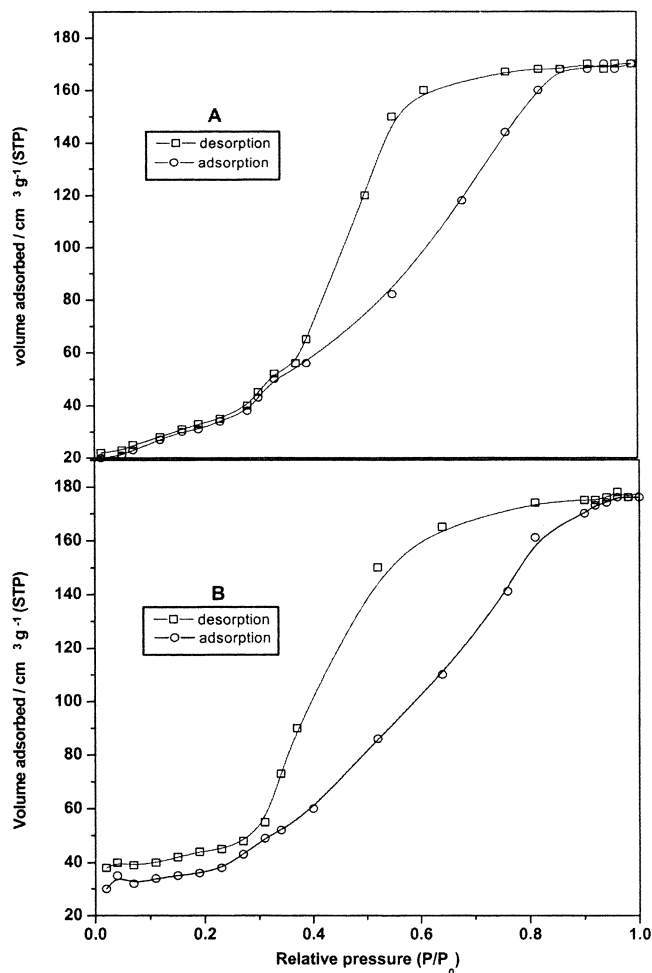


Fig. 2. N₂ adsorption isotherms of (A) Zr-TMS and (B) f-Zr-TMS-30.

triflic acid. The isotherms and pore size distributions of Zr-TMS confirm the presence of mesopores. These results are comparable with those previously reported for a mesoporous ZrO₂ [13].

Figs. 2A and 2B show the nitrogen adsorption isotherm of Zr-TMS and f-Zr-TMS-30, respectively. Both the isotherms are indicative of type IV behavior characteristic of mesoporous materials [11,13]. The hysteresis in the desorption branch clearly shows the existence of mesopores. The desorption isotherm of Zr-TMS is similar to the calcined ZrO₂ aerogels previously reported [13]. Before the functionalization (Fig. 2A) the position of the inflection in the $P/P_0 = 0.4$ to 0.83 region depends on the diameter of the mesopores (broad pore size distribution) and its sharpness indicates the uniformity of the pore size distributions. After the functionalization (Fig. 2B), the position of the inflection is changed in the $P/P_0 = 0.35$ to 0.90 region. This is indicative of a slight structural collapse in the material. However, pore size distribution analysis still indicates that mesoporosity was not lost.

Figs. 3A and 3B show the BJH pore size distributions of Zr-TMS and f-Zr-TMS-30, respectively. Zr-TMS possesses a fairly narrow distribution of mesopores centered at circa 40

Table 1
Physico-chemical properties of synthesized catalysts

Catalyst	Elemental analysis		Loading of		BET surface area ^a (m ² g ⁻¹)	Crystal ^b size (μm)	NH ₃ desorbed (mmol g ⁻¹) between temperature (°C) ^c (%)					NH ₃ chemisorbed ^d at 30 °C (mmol g ⁻¹)
	(output) (wt%)		CF ₃ SO ₃ H (wt%)				30–70	70–110	110–150	150–200	200–300	
	C	S	Input	Output								
Amorphous												
Zr(OH) ₄	–	–	–	–	80	0.35	12	27	33	20	8	0.49
≡Zr–O–SO ₂ –CF ₃ (A) ^e -5 ^f	0.7	1.00	5.0	4.7	72	0.40	11	33	37	12	6	0.81
≡Zr–O–SO ₂ –CF ₃ (A)-10	1.5	2.04	10.0	9.6	68	0.35	10	33	38	15	3	1.05
≡Zr–O–SO ₂ –CF ₃ (A)-15	1.5	2.6	15.0	12.2	63	0.38	17	29	35	15	3	1.27
≡Zr–O–SO ₂ –CF ₃ (A)-20	1.7	3.19	20.0	15.2	59	0.37	14	30	37	15	3	1.36
≡Zr–O–SO ₂ –CF ₃ (A)-25	2.0	5.16	25.0	24.2	56	0.40	13	29	38	17	3	1.53
≡Zr–O–SO ₂ –CF ₃ (A)-30	2.7	5.91	30.0	27.7	52	0.39	13	29	37	17	4	1.67
SO ₄ ²⁻ /ZrO ₂ ^g	–	3.08	10.0	7.8	101	0.45	–	–	–	–	–	1.45
Mesoporous												
Zr-TMS ^h	–	–	–	–	371	0.33	14	26	32	20	8	0.50
f-Zr-TMS-5 ^f	0.98	1.01	5.0	4.7	355	0.37	16	26	34	17	8	0.77
f-Zr-TMS-10	0.97	1.52	10.0	7.1	344	0.34	17	28	33	16	6	0.87
f-Zr-TMS-15	1.52	2.78	15.0	13.0	320	0.38	17	29	33	15	6	1.05
f-Zr-TMS-20	1.62	3.54	20.0	16.6	309	0.40	13	27	37	17	6	1.31
f-Zr-TMS-25	1.82	3.85	25.0	18.0	292	0.36	12	27	41	16	4	1.47
f-Zr-TMS-30 ⁱ	2.00	4.86	30.0	22.8	284	0.40	12	28	41	16	3	1.55

^a Measured by N₂ adsorption–desorption at –196 °C.

^b Measured by JEOL SEM (JSM-5200).

^c Percentage of acid strength distribution calculated based on NH₃ desorbed from 30 to 300 °C.

^d Total acid sites determined in the solid catalyst by NH₃ adsorption–desorption.

^e A denotes amorphous.

^f Numbers denote wt% (input) of triflic acid loading over Zr-TMS.

^g NH₃ desorbed from 30 to 600 °C.

^h Total pore volume (cm³ g⁻¹) = 0.31 and average pore diameter (Å) = 44.3 measured by N₂ adsorption isotherm.

ⁱ Total pore volume (cm³ g⁻¹) = 0.25 and average pore diameter (Å) = 34.0 measured by N₂ adsorption isotherm.

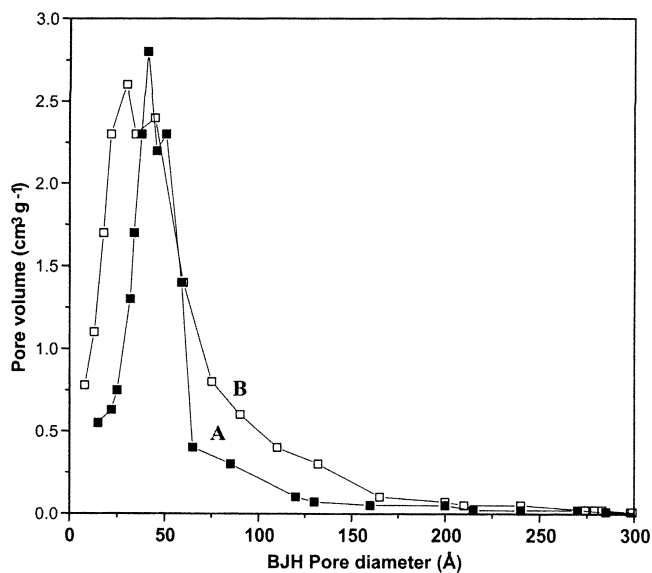


Fig. 3. BJH pore size distributions of (A) Zr-TMS and (B) f-Zr-TMS-30.

to 50 Å with some as large as 100 Å. After functionalization the distribution is clearly broadened. The material also contains smaller pores of 10 to 20 Å and the amount of larger pores (between 75 and 150 Å) is greatly increased. It is apparent that a pore formation mechanism may be in effect that differs from that of M41S materials. Pore size uniformity does not necessarily imply bi- or three-dimensional X-ray detectable ordering [11,13].

3.3. Elemental analysis study

The carbon and sulfur contents of the samples are shown in Table 1. To a first approximation, the sulfur content was assigned to the loading of triflic acid over Zr-TMS and it was observed that acid loading over Zr-TMS indeed increased with the increase in the amount of $\text{CF}_3\text{SO}_3\text{H}$ introduced. After removal of surfactant no nitrogen was detected in the elemental analysis as expected. These results were confirmed by infrared and NMR spectroscopies (see below).

3.4. Infrared spectroscopy study

The infrared spectra of Zr-TMS, f-Zr-TMS and $\equiv\text{Zr}-\text{O}-\text{SO}_2-\text{CF}_3$ (A) catalysts are shown in Figs. 4A and B, respectively. The strong and broad band between 3600 and 3200 cm^{-1} corresponds to the stretching mode of hydroxyl groups present on the surface (as $\text{Zr}(\text{OH})_4$). The weak unresolved band between 850 and 700 cm^{-1} is attributed to Zr–O stretching modes. The sharp band in the region 1650–1600 cm^{-1} is due to the bending mode of associated water molecules. The f-Zr-TMS (Fig. 4A, 5–30 wt%) and $\equiv\text{Zr}-\text{O}-\text{SO}_2-\text{CF}_3$ (A) (Fig. 4B, 5–30 wt%) spectra show additional bands (at 1296, 1184, 1043, and 601 cm^{-1}) that are absent in Zr-TMS (Fig. 4A, Zr-TMS). The broad and intense band at 1296 cm^{-1} and medium band at 1184 cm^{-1} are due to S=O stretching mode of the incorporated triflic

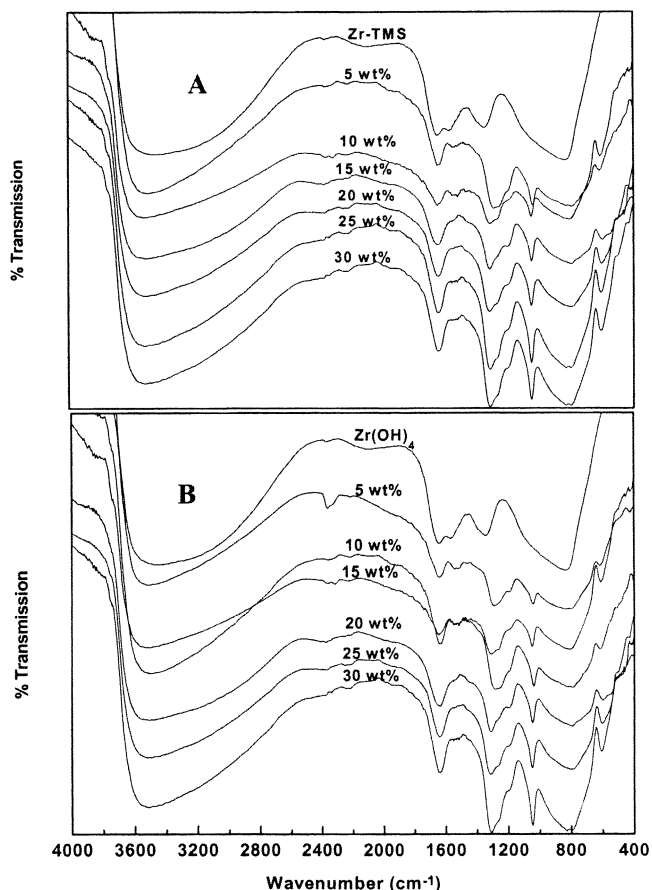


Fig. 4. IR spectrum of (A) Zr-TMS and f-Zr-TMS (5–30 wt%) and (B) $\equiv\text{Zr}-\text{O}-\text{SO}_2-\text{CF}_3$ (A) (5–30 wt%).

acid [37,38]. The C–S link in f-Zr-TMS also gives a medium band at 601 cm^{-1} . This band is assigned to the SO_2 deformation mode and a sharp band at 1043 cm^{-1} is assigned to C–F band [37,38]. Moreover, the spectra of f-Zr-TMS and $\equiv\text{Zr}-\text{O}-\text{SO}_2-\text{CF}_3$ (A) are similar to the reported silver triflate spectrum [39]. Further, from Fig. 4A, Zr-TMS, it can be seen that the stretching (3200–2800 cm^{-1}) and bending (1500–1300 cm^{-1}) modes of the methyl groups of CTMABr completely disappear after 48 h of extraction (13, 15). Thus, all these results indicate that the final material was free from surfactant and that triflic acid was functionalized onto the walls of Zr-TMS.

3.5. Solid-state ^{13}C -CP/MAS and ^{13}C -DD/MAS NMR studies

In order to confirm that the $-\text{CF}_3$ group exists in the material, the solid-state ^{13}C -CP/MAS and DD/MAS NMR spectra were recorded at 125.757 MHz at a rotational speed of 8 kHz for f-Zr-TMS-30. The DD/MAS NMR spectrum (Fig. 5) was found to be more sensitive than the CP/MAS NMR spectra, indicating the absence of a proton environment in the proximity of the carbon under observation. The quartet nature of the ^{13}C spectrum, arising due to the ^{13}C – ^{19}F scalar coupling ($J_{\text{C-F}} \approx 310$ Hz), unambiguously shows

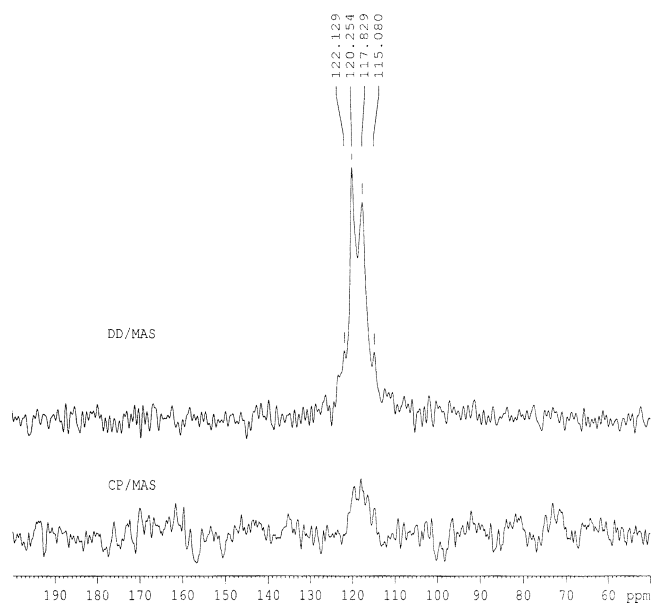


Fig. 5. Solid-state ^{13}C CP/MAS and ^{13}C DD/MAS NMR spectra of f-Zr-TMS-30.

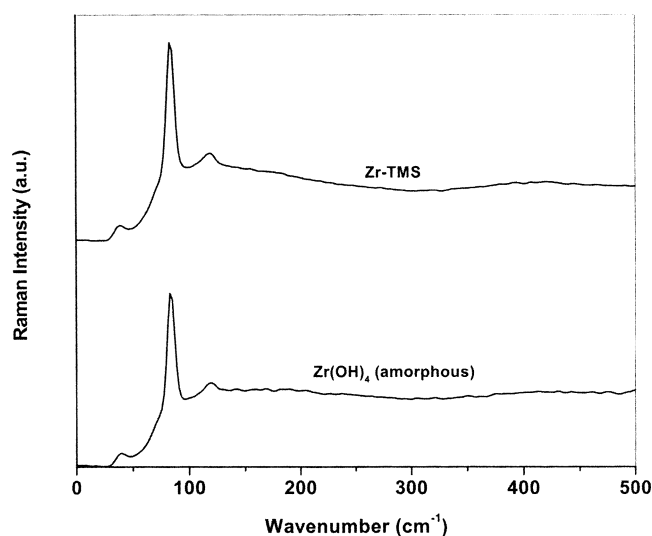


Fig. 6. FT-Raman spectra of amorphous $\text{Zr}(\text{OH})_4$ and Zr-TMS, 4 cm^{-1} , 100 scans, 50 mW.

the presence of CF_3 groups. Moreover, the chemical shift observed at ≈ 119 ppm is very close to that reported for $\text{Na-O-SO}_2\text{-CF}_3$ (≈ 120 ppm) [40]. These features indicate that the $-\text{CF}_3$ group is intact in the sample. Further, no peak corresponding to the surfactant was observed, which would normally appear in the range 10–100 ppm in the ^{13}C CP/MAS NMR spectrum.

3.6. FT-Raman analysis

Fig. 6 shows the Raman spectra of Zr-TMS and amorphous $\text{Zr}(\text{OH})_4$. The spectra of the two zirconia materials are identical, with bands at 120 cm^{-1} (w), 84 cm^{-1} (m), and 39 cm^{-1} (w). Apparently these low-frequency modes are not

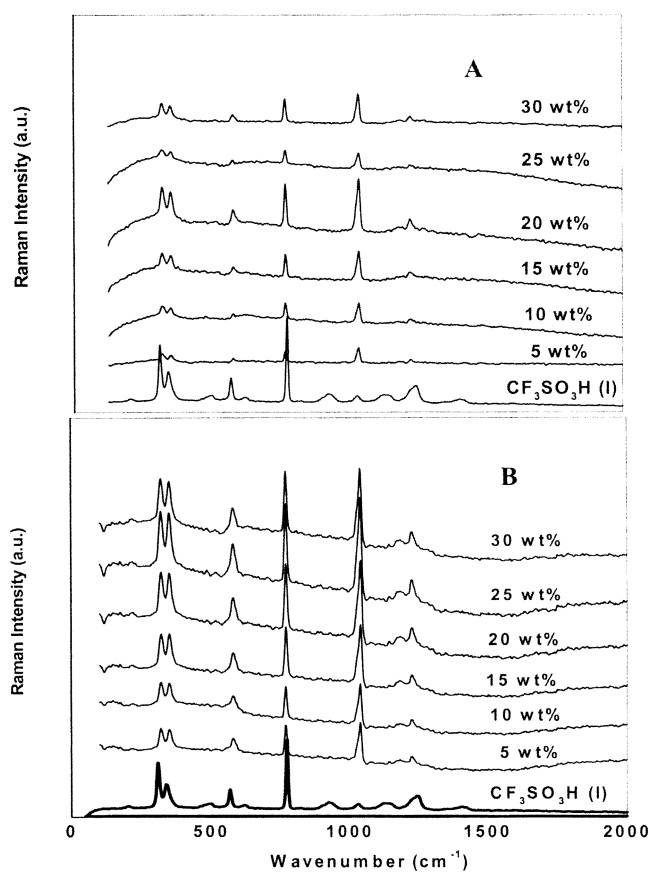


Fig. 7. FT-Raman spectra of adsorbed triflate at different acid loadings (A) on amorphous $\text{Zr}(\text{OH})_4$ and (B) on Zr-TMS. The spectra of the solid material were subtracted in each case. (4 cm^{-1} , 100 scans, 50 mW). The spectrum of liquid triflic acid is also shown in each case for comparison.

sensitive to the presence or absence of mesopores. Fig. 7A shows the Raman spectra of f-Zr-TMS with triflic acid loadings between 5 and 30 wt%. The spectrum of the Zr-TMS support was subtracted from each. Also shown is the spectrum of liquid triflic acid. Clearly, the spectra of all the f-Zr-TMS samples are very similar to each other and to that of liquid trifluoromethanesulfonic acid. No bands appear in the spectra of the f-Zr-TMS samples that do not appear in the spectrum of the acid itself. Only small peak shifts exist for some bands on the supported samples relative to the liquid acid. These will be discussed in detail later. Comparing Fig. 7A, 5–30 wt%, one observes that the intensity of each band increases with increased loading of triflate. Fig. 7A, 20 wt%, is somewhat anomalous and may indicate that the sample actually contains more than 20 wt% triflate. Elemental analysis in fact revealed that the sulfur content was lower than 20 wt% (16.6 wt%). According to Table 1 the actual change in S content between spectra 7A, 20–30 wt%, was smaller than theoretically calculated (13–22.8 wt% rather than 15–30 wt%). Fig. 7B shows the spectra for the $\equiv\text{Zr-O-SO}_2\text{-CF}_3$ (A) samples. Again the spectrum of the support was subtracted. These spectra are again very similar to that of the liquid acid.

Table 2
Compilation of Raman bands measured (cm^{-1}) for f-Zr-TMS, $\equiv\text{Zr-O-SO}_2\text{-F}_3$ (A) and for liquid $\text{CF}_3\text{SO}_3\text{H}$

f-Zr-TMS	$\equiv\text{Zr-O-SO}_2\text{-CF}_3$ (A)	$\text{CF}_3\text{SO}_3\text{H}$ (liq.)	Assignment [41] ^a
	This study	Literature [41] ^a	
–	–	2999	$\nu(\text{OH}) A'$ [42]
1412	1396	1410	$\nu_{\text{as}}(\text{SO}_2) A''$
1256	1266	1248	$\nu_{\text{s}}(\text{SO}_2) A'$
1229	1228	~ 1228	$\nu_{\text{d}}(\text{CF}_3) E$
–	1185	1151	$\nu_{\text{s}}(\text{CF}_3) A_1$
–	–	1130	$\delta(\text{SOH}) A'$
1038	1040	1030	$\nu_{\text{s}}(\text{S-O}_3^-)$ [42,43]
929	924	929	$\nu(\text{SO(H)}) A'$
768	769	773	$\delta_{\text{s}}(\text{CF}_3) A'$ [41], $\nu(\text{CS}) A'$ [42]
~ 620	619	619	$\delta(\text{SO}_2 \text{ bend}) A'$
576	578	568	$\delta_{\text{d}}(\text{CF}_3) E$
513	518	499	$\delta(\text{SO(H) wag}) A'$
~ 480	492	478 (sh)	$\delta(\text{SO}_2 \text{ rock}) A''$
350	351	339	$\delta(\text{SCF}_3 \text{ wag}) A'$
319	321	309	$\nu(\text{CS}) A'$ [41], $\text{CF}_3 \text{ wag } A''$ [42]
~ 223	213	202	$\rho(\text{CF}_3) E$

The band assignments were made previously [41,42] and apply to the liquid acid molecule only.

^a Assignments were made assuming that the $\text{CF}_3\text{SO}_3\text{H}$ molecule belongs to the point group C_s , however, with local C_{3v} symmetry (CF_3 group).

The peak data from Figs. 7A and B are compiled in Table 2. Also listed are previously published data regarding the Raman spectrum of liquid trifluoromethanesulfonic acid and the band assignments previously made for this molecule [41,42]. As shown in Table 2, excellent agreement exists between the measured and the previously reported Raman spectra of liquid triflic acid. The assignments are from the work of Katsuhara et al. [41] who were the first to measure and assign the complete spectrum between 1500 and 0 cm^{-1} . They assumed that the $\text{CF}_3\text{SO}_3\text{H}$ molecule belonged to the point group C_s with, however, local C_{3v} symmetry (the CF_3 group). They also assumed that this group was free to rotate around the C–S bond. The most relevant bands for this study are the SOH deformation mode at 1122 cm^{-1} and the symmetric and asymmetric stretching modes of SO_2 (at 1248 and 1410 cm^{-1} , respectively). The symmetric stretching band of the triflate anion (CF_3SO_3^-) is also included in Table 2 (1034 cm^{-1} [42], 1038 cm^{-1} [43]). This peak was not observed in very pure acid since there is very little dissociation. We observed a small band at 1030 cm^{-1} . Since no attempt was made to purify the acid or to keep it totally dry, trace water obviously led to some dissociation in our case. Finally, the OH stretching frequency, previously reported at 2997 cm^{-1} [42], was observed at 2999 cm^{-1} in this study. Previous work on bulk samples of metal sulfonate salts [43] showed that the sulfonate oxygen atoms were in equivalent, symmetric positions. Normal coordinate analyses of IR and Raman spectra indicated that the CX_3SO_3^- anions (X = H, D, F, Cl) had C_{3v} symmetry in which the three oxygen atoms coordinate in an equivalent manner to a metal ion with three-fold rotational symmetry about the C–S bond. Essentially the sulfonate group acts as a tripod.

The C_{3v} point group has 18 normal vibrational modes that can be classified by the symmetry types: $\Gamma_{\text{vib}} = 5A' + A'' + 6E$. All modes, excepting the A'' mode, are both IR and Raman active. Hall and Hansma [43] studied the adsorption and orientation of sulfonic acids on alumina using inelastic tunneling spectroscopy and found that sulfonate groups also bind through three equivalent oxygen atoms in a tridentate form on this surface. The four possible binding modes of CF_3SO_3^- (a) monodentate, (b) bidentate, (c) tridentate, and (d) tridentate (distorted) can be distinguished by their spectra in the following manner. The lowered symmetry of monodentate sulfonates (bound via only one oxygen) leads to splitting of the three degenerate S-O_3^- stretching modes and produces a spectrum containing three distinct modes spanning about 500 cm^{-1} , centered around 1100 cm^{-1} . Bidentate ligands (bound via two oxygen atoms) also produce three different S–O stretching modes centred around 1150 to 1250 cm^{-1} and separated by at least 300 cm^{-1} . The totally symmetric tridentate sulfonate group (C_{3v}) has only two different S–O stretching modes, the symmetric stretch ν_{s} and the doubly degenerate asymmetric stretch ν_{a} . Slight distortion from C_{3v} symmetry results in loss of degeneracy of these two modes resulting in two asymmetric S–O bands slightly split ($\leq 32 \text{ cm}^{-1}$) about their degenerate position. The vibrations involving the S-O_3^- group for the CF_3SO_3^- anion and their measured frequencies (using IR and Raman) are shown in Table 3. In a recent previous publication [44] some of us reported the transmission infrared spectrum of f-Zr-TMS. The spectrum contained four bands not present in the IR spectrum of the Zr-TMS support. These bands appeared at 1296 cm^{-1} (vs), 1184 cm^{-1} (m), 1043 cm^{-1} (vs), and 601 cm^{-1} (m, br). The first two bands were previously assigned to ν_{a} and ν_{s} of the $\text{CF}_3\text{S-O}_3^-$ group

Table 3
Vibrational modes of S-O_3^- group (assuming C_{3v} symmetry) for CF_3SO_3^- and their measured IR and Raman frequencies (cm^{-1})

Mode	IR [43]	Raman [43]	Raman [this study]	
			On Zr-TMS	On amorphous Zr(OH)_4
$\nu_s(\text{S-O}_3^-)$ A'	1019–1049 (s-vs)	1038 (s-vs) p	1038	1041
$\nu_a(\text{S-O}_3^-)$ E	1152–1194 (s-vs)	1188 (vw) dp	–	1185
$\delta_s(\text{S-O}_3^-)$ A'	630–676 (s-vs, br)	635 (s) p	~ 620	619
$\delta_a(\text{S-O}_3^-)$ E	515–531 (w-s)	520 (vw) dp	513	518
$\rho_a(\text{S-O}_3^-)$ E	350–356 (w-s)	353–359 (m) dp	350	351

bound to the surface. However, a more careful examination of the spectrum shows an unresolved shoulder at 1200 cm^{-1} . As shown in Table 3, this band should be assigned to $\nu_a(\text{CF}_3\text{S-O}_3^-)$ E. This very weak mode was observed at 1038 cm^{-1} on the $\equiv\text{Zr-O-SO}_2\text{-CF}_3$ (A) samples (see Table 2). The band at 1296 cm^{-1} should be assigned to $\nu_a(\text{C-F}_3)$ E. According to [43], this band has been observed in the IR between 1259 and 1280 cm^{-1} (vs, br) and at 1285 cm^{-1} (vw, dp) in some Raman spectra. Very weak bands were detected at 1256 and 1266 cm^{-1} in the spectra of the f-Zr-TMS and $\equiv\text{Zr-O-SO}_2\text{-CF}_3$ (A) materials, respectively. In addition, the band previously reported at 601 cm^{-1} in the IR spectrum is more probably two unresolved bands. Table 3 shows that the symmetric deformation mode of triflate anion, $\delta_s(\text{S-O}_3^-)$ A' appears at slightly higher frequencies (630 – 676 cm^{-1} (s-vs, br)) in the IR, and at 635 cm^{-1} (s, p) in the Raman. Bands were observed at $\sim 620 \text{ cm}^{-1}$ on both the amorphous and the mesoporous samples. The second component of the band is probably due to the asymmetric deformation mode of the CF_3 group [$\delta_d(\text{C-F}_3)$ E]. As reported in [43], this mode appears between 577 and 591 cm^{-1} (vw-s) in the IR, and at 580 cm^{-1} in the Raman (vw, dp). Bands were observed at 576 cm^{-1} in this study.

3.7. Ammonia adsorption–desorption study

Experimental data obtained using the Hammett acidity function have shown that triflic acid and perfluorinated acid resins are superacids with H_o values between -12 and -14 [45,46]. However discrepancies and uncertainties in the practical applications of Hammett acidity made us look for other methods to determine the acid strength of our functionalized materials. Marziano et al. [36] and Corma et al. [47] used potentiometric titration with standardized NaOH and ammonia TPD measurements to obtain the total acidity and the distribution of their acid strengths of triflate and $\text{SO}_4^{2-}/\text{ZrO}_2$ materials, respectively. Hence, the ammonia TPD technique was used to measure the acidity of the synthesized catalysts.

In addition to the total number of acid sites, a quantitative distribution of acid strengths of the sites on the functionalized materials was obtained by measuring the amounts in five arbitrarily defined temperature regions during the ammonia TPD experiment (between 30 and 70°C , 70 and 110°C , 110 and 150°C , 150 and 200°C , and 200 and 300°C). Since the functionalized materials are covalently

bonded to the solid support, it could not be treated above 300°C (above this temperature triflic acid is lost from the solid support [20,26,27,36]). Table 1 shows the total number of acid sites (determined via NH_3 chemisorbed at 30°C) of Zr-TMS, f-Zr-TMS and $\equiv\text{Zr-O-SO}_2\text{-CF}_3$ (A). The quantitative distributions of the acid sites (in the 5 regions) are also shown.

The total number of acid sites on the catalysts was found to increase proportionally with increased loading of triflic acid supported on Zr-TMS. The same trend of increasing the total number of acid sites with increasing triflic acid loading was observed in the $\equiv\text{Zr-O-SO}_2\text{-CF}_3$ (A) catalysts (see Table 1). A larger number of acid sites were observed for the amorphous catalyst ($\equiv\text{Zr-O-SO}_2\text{-CF}_3$ (A)-30) than for the mesoporous catalyst (f-Zr-TMS-30). This is consistent with the results of elemental analysis (see Table 1).

The total number of acid sites on the Zr-TMS was found to be 0.50 mmol g^{-1} ; the Brønsted acid sites are formed by the hydroxyl groups that exist in the Zr-TMS material. The total amount of NH_3 chemisorbed at 30°C was 0.77 mmol g^{-1} for f-Zr-TMS-5, and 1.55 mmol g^{-1} for f-Zr-TMS-30. The total number of acid sites on $\text{SO}_4^{2-}/\text{ZrO}_2$ (measured between 30 and 600°C) was found to be 1.45 mmol g^{-1} . Silica-supported triflic acid showed superacid character (i.e., the acidity was greater than that of $100\% \text{ H}_2\text{SO}_4$ [26]. Triflic acid alone is also known to be a superacid [20].

Further, the acid strength distribution (in %) of Zr-TMS, f-Zr-TMS, amorphous Zr(OH)_4 , and $\equiv\text{Zr-O-SO}_2\text{-CF}_3$ (A) are given in Table 1. The results of ammonia TPD measurements reveal that the total acidity (mmol g^{-1} at 30°C) increases with the increase in loading of triflic acid over amorphous Zr(OH)_4 and Zr-TMS. However, the acid strength distribution (measured in five steps) remains nearly unchanged except between 110 and 150°C . It is observed that the percentage of the acid sites (between 110 and 150°C) increases from 33 to about 38% , and 32 to 41% when the triflic acid loading was increased from 0 to $30 \text{ wt}\%$ over amorphous Zr(OH)_4 and Zr-TMS, respectively.

3.8. Scanning electron microscopic study

The particle size and morphology of Zr-TMS and f-Zr-TMS-30 were studied by SEM. SEM micrographs of Zr-TMS (Fig. 8A) and f-Zr-TMS-30 (Fig. 8B) are typical of ordered ZrO_2 - [48] and MCM-41- [49] type materials exhibit-

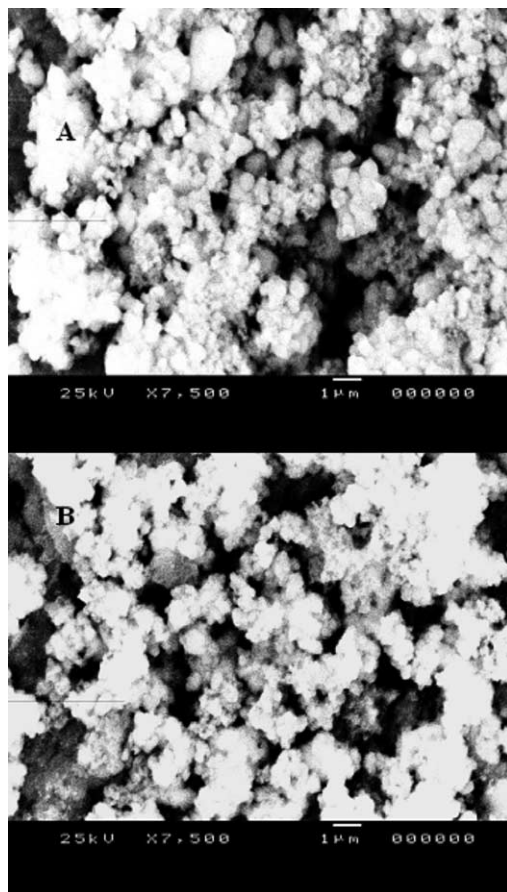


Fig. 8. Scanning electron micrographs of (A) Zr-TMS and (B) f-Zr-TMS-30.

ing the winding-worm type. It is noteworthy that previous authors have reported mesoporous zirconia to be very disordered [11]. Zr-TMS consisted of ordered particles (winding-worm type) of approximately $0.33\ \mu\text{m}$ in size. The particle size of f-Zr-TMS-30 was slightly larger (approximately $0.4\ \mu\text{m}$). The particles appeared to be of a distorted winding-worm type. It appears that functionalization alters the particle size to some extent. The increase in the particle size with the increase of $\text{CF}_3\text{SO}_3\text{H}$ loading is attributed to anchoring of triflic acid on Zr-TMS. This decrease in ordering and crystallinity was also observed by XRD.

3.9. Transmission electron microscopic study

The samples were prepared for TEM analysis by sonification in isopropanol followed by deposition on carbon-coated copper grids. Transmission electron micrographs of Zr-TMS (Fig. 9A) and f-Zr-TMS-30 (Fig. 9B) reveal that these materials have a highly porous nature and contain either disordered hexagonal phases or pseudo-hexagonal arrays. These results are in good agreement with the earlier studies of Zr-TMS [50,51].

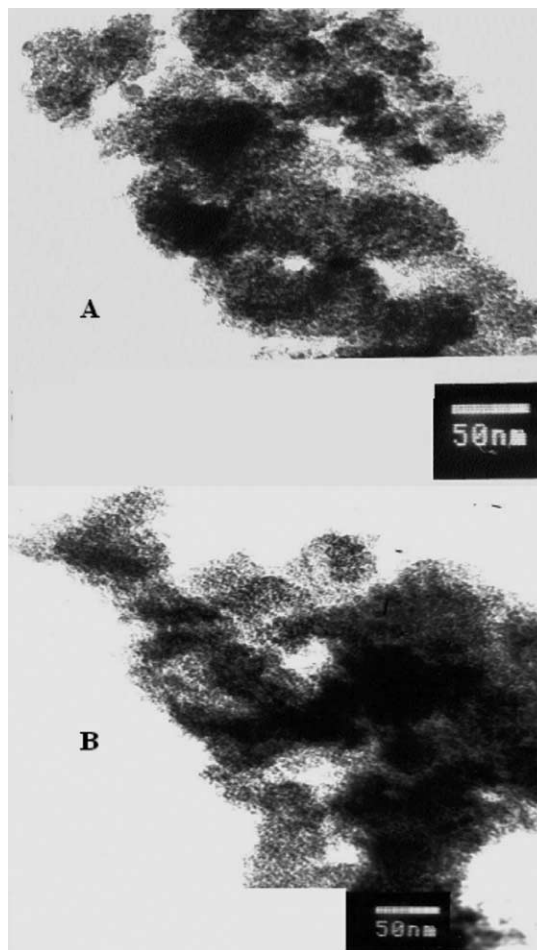


Fig. 9. Transmission electron micrographs of (A) Zr-TMS and (B) f-Zr-TMS-30.

3.10. Thermal analysis (TG, DTA, and DTG)

Thermal analysis of all synthesized catalysts showed similar results. Figs. 10A and 10B show typical TG, DTA, and DTG profiles measured for Zr-TMS and f-Zr-TMS-30 samples, respectively. The TG curve of Zr-TMS shows three stages of weight loss. The weight loss (endothermic) between 70 and $200\ ^\circ\text{C}$ corresponds to the loss of loosely bound water (desorption of adsorbed water) [52] and residual butanol (the latter was used as solvent in the synthesis mixture). Further, the weight loss between 200 and $400\ ^\circ\text{C}$ corresponds to the decomposition of $\text{Zr}(\text{OH})_4$ into ZrO_2 [11,13]. A slight decrease at about $450\ ^\circ\text{C}$ in the TG curve and a corresponding sharp exothermic peak at the same temperature in the DTA curve are indicative of an additional phase coexisting with zirconia. This may be a quasi-amorphous tetragonal phase produced in the decomposition process of $\text{Zr}(\text{OH})_4$ [53]. No further weight losses were observed above $650\ ^\circ\text{C}$. At this point the residue is anhydrous ZrO_2 .

The TG curve of f-Zr-TMS-30 (Fig. 10B) shows four stages of weight loss as described above. The decrease between 70 and $200\ ^\circ\text{C}$ corresponds to the loss of loosely

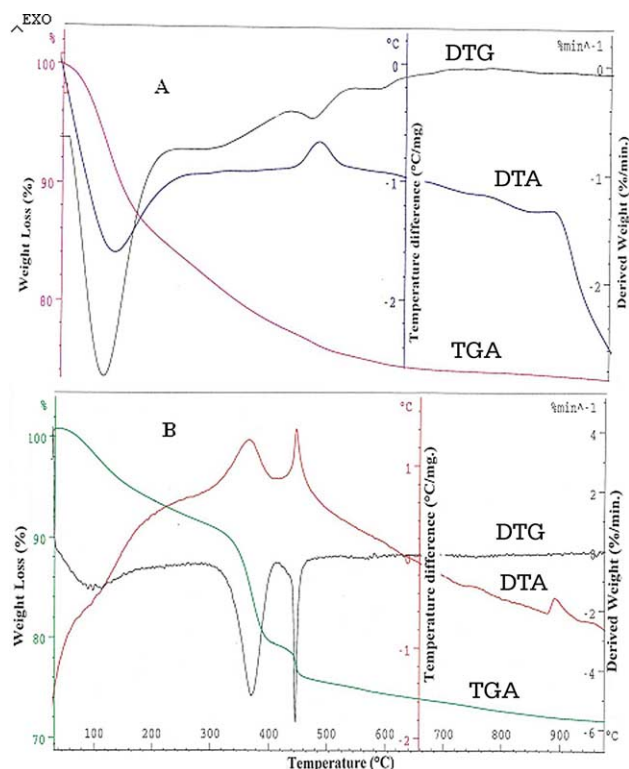


Fig. 10. Thermogravimetric differential thermal analysis (TG, DTA, and DTG) profiles of (A) Zr-TMS and (B) f-Zr-TMS-30.

bound water and residual butanol. The large weight losses between 320 and 400 °C [28] and between 400 and 440 °C correspond to the loss of the trifluoromethane sulfonate ($\text{O-SO}_2\text{-CF}_3$) group from the zirconia surface and to the complete phase change of Zr(OH)_4 to ZrO_2 , respectively. Hence these functionalized materials cannot be treated above 300 °C.

Differential thermal gravimetric analysis of the catalysts agreed well with the results obtained by TG-DTA. Fig. 10A shows the DTG profile of the Zr-TMS catalyst. Two endothermic peaks were observed (at about 110 and 450 °C) for Zr-TMS whereas three endothermic peaks were observed (at about 100, 370, and 440 °C) for f-Zr-TMS-30 (Fig. 10B). The endothermic peak at 360 °C corresponds to the loss of trifluoromethanesulfonate. The sharp endothermic peak at 440 °C is attributed to the additional phase and the phase change of zirconia. In addition, a sharp exothermic peak at about 900 °C in the DTA curve corresponds to the crystallization of material and the phase change from tetragonal to monoclinic and it is also observed in Zr-TMS (Fig. 10A).

3.11. Catalytic activity

The catalytic activity of the synthesized materials was examined in the acetalization of ethylacetoacetate with ethylene glycol to fructose, and in the benzylation of biphenyl with benzoyl chloride to 4-PBP in batch reactors at 100 °C for 1 h and 170 °C for 6 h, respectively. Both reactions were

also carried out using $\text{SO}_4^{2-}/\text{ZrO}_2$ and triflic acid for comparison.

3.12. Acetalization of ethylacetoacetate

The results of acetalization of ethylacetoacetate to fructose are given in Table 4. Under similar reaction conditions, the f-Zr-TMS catalysts were more active than Zr-TMS and comparable to $\text{SO}_4^{2-}/\text{ZrO}_2$ and $\equiv\text{Zr-O-SO}_2\text{-CF}_3$ (A). The Zr-TMS and amorphous Zr(OH)_4 showed 21 and 18 wt% conversion of EAA, respectively, due to the limited number of acid sites. However, in terms of selectivity amorphous Zr(OH)_4 gave 97 wt% to fructose whereas Zr-TMS was 100 wt% selectivity to fructose. This higher selectivity is attributed to the presence of well-defined pores. Since the acidity of the functionalized mesoporous and the amorphous catalysts are similar with respect to the triflic acid loading (Table 1), both series of catalysts showed more or less similar conversion of EAA. The EAA conversion was 82 wt% for f-Zr-TMS-5 and 93 wt% for f-Zr-TMS-30. Further, the EAA conversion over $\equiv\text{Zr-O-SO}_2\text{-CF}_3$ (A)-5 and $\equiv\text{Zr-O-SO}_2\text{-CF}_3$ (A)-30 was 83 and 92 wt%, respectively. All the f-Zr-TMS catalysts showed the conversion of EAA between 82 and 93 wt% with 100 wt% selectivity to fructose (Table 4). The selectivity of the $\equiv\text{Zr-O-SO}_2\text{-CF}_3$ (A) catalysts to fructose was much poorer (between 64 and 82 wt%) than over the f-Zr-TMS catalysts. $\text{SO}_4^{2-}/\text{ZrO}_2$ showed 93 wt% conversion of EAA and 90 wt% selectivity to fructose. The lower selectivity of $\text{SO}_4^{2-}/\text{ZrO}_2$ may be correlated due to its nonuniform pore size, low porosity, and smaller surface area. Pure $\text{CF}_3\text{SO}_3\text{H}$ showed higher conversion (95 wt%) than all the catalysts, with a selectivity of 74 wt%. The homogeneous medium of strong acid and the water formed during this reaction can cause the hydrolysis of the ester, producing the corresponding EDDBA (3,3-ethylenedioxybutanoic acid). The formation of this product not only reduces the yield of fructose, but also it can alter the organoleptic characteristics of the final product. The turnover frequency (TOF) was calculated as number of moles of EAA converted per moles of sulfur per hour. Since the conversions were almost the same in all the cases with respect to the loading of triflic acid, TOFs was found to be approximately similar for both types of catalysts (Table 4). The TOFs (in $\text{mol}^{-1}\text{S h}^{-1}$) for f-Zr-TMS-5, f-Zr-TMS-30, and $\equiv\text{Zr-O-SO}_2\text{-CF}_3$ (A)-5 and $\equiv\text{Zr-O-SO}_2\text{-CF}_3$ (A)-30 were 259 and 61.2 and 265.6 and 49.8, respectively. The TOFs of triflic acid and $\text{SO}_4^{2-}/\text{ZrO}_2$ were 54.0 and 96.9, respectively.

3.13. Benzylation of biphenyl

The results for the benzylation reaction of BP to 4-PBP are given in Table 5. As in the acetalization reaction, due to the limited acidity, both Zr-TMS and amorphous Zr(OH)_4 showed comparable conversion of BP, 3.2 and 3.1 wt%, respectively. Further, the biphenyl conversion dramatically

Table 4
Acetalization of ethylacetoacetate^a

Catalyst	Conversion of EAA (wt%)	TOF ^b (h ⁻¹ mol ⁻¹ S)	Product distribution (wt%) ^c	
			EDBA	Fructose
Amorphous				
Amorphous-Zr(OH) ₄	18.0	–	3	97
≡Zr–O–SO ₂ –CF ₃ (A)-5	83.0	265.6	36	64
≡Zr–O–SO ₂ –CF ₃ (A)-10	83.0	130.2	18	82
≡Zr–O–SO ₂ –CF ₃ (A)-15	89.0	105.5	27	73
≡Zr–O–SO ₂ –CF ₃ (A)-20	94.0	94.1	21	79
≡Zr–O–SO ₂ –CF ₃ (A)-25	89.0	55.2	22	78
≡Zr–O–SO ₂ –CF ₃ (A)-30	92.0	49.8	35	65
CF ₃ SO ₃ H ^d	95.0	54.0	26	74
SO ₄ ²⁻ /ZrO ₂	93.0	96.6	10	90
Mesoporous				
Zr-TMS	21.0	–	0	100
f-Zr-TMS-5	82.0	259.0	0	100
f-Zr-TMS-10	87.0	183.0	0	100
f-Zr-TMS-15	88.0	101.3	0	100
f-Zr-TMS-20	88.0	79.5	0	100
f-Zr-TMS-25	91.0	75.6	0	100
f-Zr-TMS-30	93.0	61.2	0	100

^a Reaction conditions: catalyst (g) = 0.1; ethylacetoacetate (mmol) = 10; ethylene glycol (mmol) = 10; reaction time (h) = 1; reaction temperature (°C) = 100; toluene (g) = 25.

^b TOF is given as moles of EAA transformed per hour per mole of sulfur.

^c EDDBA, 3,3-ethylenedioxybutanoic acid; Fructose, ethyl 3,3-ethylenedioxybutyrate.

^d Catalyst (g) = 0.125; reaction time (h) = 1.

Table 5
Benzoylation of biphenyl^a

Catalyst	Conversion of biphenyl (wt%)	TOF ^b (10 ⁻¹ h ⁻¹ mol ⁻¹ S)	Product distribution (wt%) ^c	
			2-PBP	4-PBP
Amorphous				
Amorphous-Zr(OH) ₄	3.1	–	0	100
≡Zr–O–SO ₂ –CF ₃ (A)-5	5.0	5.34	3	97
≡Zr–O–SO ₂ –CF ₃ (A)-10	10.2	5.55	2	98
≡Zr–O–SO ₂ –CF ₃ (A)-15	15.5	6.36	2	98
≡Zr–O–SO ₂ –CF ₃ (A)-20	16.0	5.34	4	96
≡Zr–O–SO ₂ –CF ₃ (A)-25	19.1	4.2	3	97
≡Zr–O–SO ₂ –CF ₃ (A)-30	20.5	3.7	2	98
CF ₃ SO ₃ H ^d	63.7	54.3	7	93
SO ₄ ²⁻ /ZrO ₂	7.2	0.98	0	100
Mesoporous				
Zr-TMS	3.2	–	0	100
f-Zr-TMS-5	22.0	23.2	0	100
f-Zr-TMS-10	27.0	21.9	0	100
f-Zr-TMS-15	31.5	12.1	0	100
f-Zr-TMS-20	35.0	10.5	0	100
f-Zr-TMS-25	37.0	10.2	0	100
f-Zr-TMS-30	41.0	9.0	0	100

^a Reaction conditions: catalyst (g) = 0.5; biphenyl (mmol) = 10; benzoyl chloride (mmol) = 10; reaction time (h) = 6; reaction temperature (°C) = 170; nitrobenzene (ml) = 20.

^b TOF is given as moles of BP transformed per hour per mole of sulfur.

^c 2-PBP, 2-phenylbenzophenone; 4-PBP, 4-phenylbenzophenone.

^d Catalyst (g) = 0.125; reaction time (h) = 3.

increased after the functionalization of triflic acid over Zr-TMS. All the f-Zr-TMS catalysts showed higher conversion of BP with 100 wt% selectivity to 4-PBP. The conversion of BP over the f-Zr-TMS catalysts was between 22 and 41 wt% when the triflic acid loading was increased from 5 to

30 nominal wt%. In the same manner, the conversion of BP over the ≡Zr–O–SO₂–CF₃ (A) catalysts was between 5 and 20 wt% for nominal loadings of triflic acid increasing from 5 to 30 wt%. In terms of selectivity, the f-Zr-TMS catalysts showed 100 wt% to 4-PBP whereas the ≡Zr–O–SO₂–CF₃

Table 6
Recycling of f-Zr-TMS-30 in acetalization reaction^a

Cycle	Elemental analysis ^b (wt%)		Conversion of EAA (wt%)	TOF ^c (h ⁻¹ mol ⁻¹ S)	Selectivity to fructose (wt%)
	C	S			
Fresh	2.0	4.86	93.0	61.2	100
First recycle	1.96	4.79	86.0	61.8	100
Second recycle	1.92	4.71	86.0	68.7	100

^a Reaction conditions: catalyst (g) = 0.1; ethylacetoacetate (mmol) = 10; ethylene glycol (mmol) = 10; reaction time (h) = 1; toluene (g) = 25; reaction temperature (°C) = 100.

^b Elemental analysis by EA1108 elemental analyzer (Carlo Erba).

^c TOF is given as moles of EAA transformed per hour per mole of sulfur.

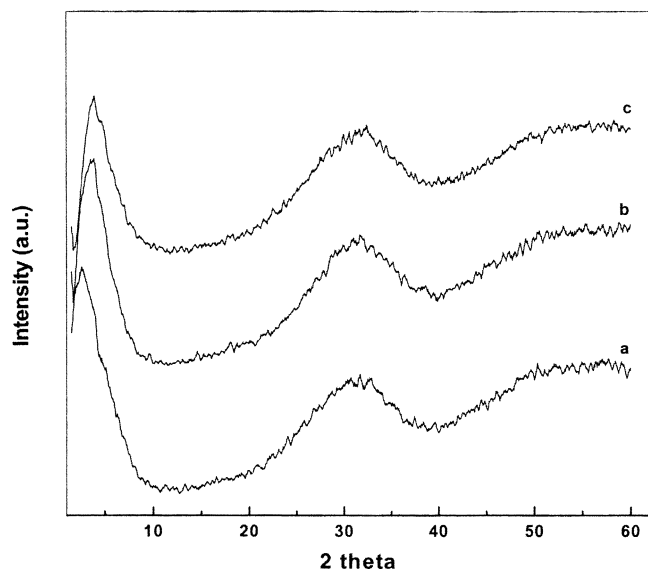


Fig. 11. XRD patterns of fresh and recycled catalysts (a) f-Zr-TMS-30 (fresh), (b) after one recycle, and (c) after two recycles.

(A) catalysts produced a small amount of 2-PBP due to its nonporous structure. Triflic acid and $\text{SO}_4^{2-}/\text{ZrO}_2$ showed 63.7 and 7.2 wt% conversions of BP, respectively. The selectivity to 4-PBP over $\text{CF}_3\text{SO}_3\text{H}$ was only 93 wt% due to its nonshape-selective nature. These results demonstrate that the BP benzylation reaction essentially needs a porous catalyst with uniform pore size and higher acidity. The TOFs were calculated as the number of moles of BP converted per mole of sulfur per hour. TOFs (in $10^{-1} \text{ mol}^{-1} \text{ S h}^{-1}$) of BP conversion over f-Zr-TMS-5, f-Zr-TMS-30, $\equiv\text{Zr}-\text{O}-\text{SO}_2-\text{CF}_3$ (A)-5, and $\equiv\text{Zr}-\text{O}-\text{SO}_2-\text{CF}_3$ (A)-30 were 23.2, 9.0, 5.34, and 3.7, respectively. The TOFs (in $10^{-1} \text{ mol}^{-1} \text{ S h}^{-1}$) of $\text{CF}_3\text{SO}_3\text{H}$ and $\text{SO}_4^{2-}/\text{ZrO}_2$ were 54.3 and 0.98, respectively.

3.14. Catalyst recycling study

Recycle of the synthesized catalysts was studied in the acetalization reaction using f-Zr-TMS-30 in order to check the stability and activity of recycled catalysts (Table 6). Three reaction cycles (fresh and two recycles) were carried out under similar reaction conditions, using the same catalyst. Elemental analysis (Table 6) and XRD analysis (Fig. 11)

showed that both sulfur content and catalyst crystallinity decreased after each cycle. The conversion of EAA decreased to some extent on recycling (from 93 to 86 wt%), whereas the selectivity to fructose did not change. The loss of sulfur and the decrease in the crystallinity of the catalyst were the likely causes of the decrease in catalytic activity.

4. Conclusions

In conclusion, Zr-TMS catalysts have been synthesized based on the sol-gel method by using CTMABr and TMAOH. The template was extracted from the synthesized materials by using ethanol and HCl. The extracted Zr-TMS was successfully functionalized with triflic acid by postsynthesis treatment to obtain covalently bonded f-Zr-TMS catalysts. Various loadings of triflic acid over Zr-TMS were prepared by varying the molar ratios of $\text{Zr}(\text{OC}_4\text{H}_9)_4$, CTMABr, TMAOH, H_2O , and $\text{CF}_3\text{SO}_3\text{H}$. Functionalized amorphous $\equiv\text{Zr}-\text{O}-\text{SO}_2-\text{CF}_3$ catalysts were also synthesized and characterized for comparison. The catalysts were characterized by various physico-chemical techniques such as XRD, N_2 adsorption-desorption, FTIR, FT-Raman, elemental analysis, ^{13}C DD/MAS NMR, TPD of NH_3 , SEM, TEM, and thermal analysis. BET surface area and pore size distribution results were in general agreement with previous values reported for mesoporous ZrO_2 . The NH_3 -TPD measurements showed that the catalysts were highly acid. ^{13}C DD/MAS NMR revealed that the $-\text{CF}_3$ group remained intact in the material. FT-Raman analysis demonstrated that the triflic acid was bonded in an identical fashion on both amorphous $\text{Zr}(\text{OH})_4$ and Zr-TMS at all loadings. Triflate ligands bound via 3 equivalent oxygen atoms to zirconium atoms forming tripod structures. TEM studies teach that the material contained disordered channels, unlike MCM-41 mesoporous molecular sieves. Acetalization of EAA to fructose and benzylation of BP to 4-PBP reactions were performed on f-Zr-TMS, $\equiv\text{Zr}-\text{O}-\text{SO}_2-\text{CF}_3$ (A), triflic acid, and $\text{SO}_4^{2-}/\text{ZrO}_2$. f-Zr-TMS catalysts were found to be the most active and selective in both reactions due to their mesoporosity and to an increase in the number of acid sites with the “right” acid strength. The stability and recycle effect of the catalysts were checked in the acetalization reaction by using f-Zr-TMS-30. No major loss of activity was observed after two recycles,

but a decrease of the sulfur content and catalyst crystallinity was observed.

Acknowledgments

The authors are thankful to Drs. C. Gopinathan, S.S. Desphande, P.R. Rajamohanam, H.S. Soni, N.E. Jacob, A.A. Belhekar, R. Parischa, S. Violet, R. Marimuthu, and C. Venkatesan for their valuable contribution and cooperation in characterizing the catalysts.

References

- [1] Y.D. Xia, W.M. Hua, Y. Tang, Z. Goa, *Chem. Commun.* (1999) 1899.
- [2] T. Jin, T. Yamaguchi, K. Tanabe, *J. Phys. Chem.* 90 (1986) 4797.
- [3] M. Hino, K. Arata, *J. Chem. Soc., Chem. Commun.* (1979) 1148.
- [4] A. Corma, *Chem. Rev.* 95 (1995) 559.
- [5] Z. Liu, W. Ji, L. Dong, Y. Chen, *Mater. Chem. Phys.* 56 (1998) 134.
- [6] D.M. Antonelli, J.Y. Ying, *Angew. Chem., Int. Ed. Engl.* 35 (1996) 426.
- [7] D.M. Antonelli, J.Y. Ying, *Chem. Mater.* 8 (1996) 874.
- [8] D. Terribile, A. Trovarelli, J. Llorca, C. de Leitenburg, G. Dolcetti, *J. Catal.* 178 (1998) 299.
- [9] A. Sayari, P. Liu, *Micropor. Mater.* 12 (1997) 149.
- [10] G.D. Yadav, J.J. Nair, *Micropor. Mesopor. Mater.* 33 (1999) 1.
- [11] V.I. Parvulescu, H. Bonnemann, V. Parvulescu, B. Endruschat, A.Ch.W. Rufinska, B. Tesche, G. Poncelet, *Appl. Catal. A* 214 (2001) 273.
- [12] J.A. Knowles, M.J. Hudson, *J. Chem. Soc., Chem. Commun.* (1995) 2083.
- [13] M.J. Hudson, J.A. Knowles, *J. Mater. Chem.* 6 (1) (1996) 89.
- [14] G. Pacheco, E. Zhao, E.D. Valdes, A. Garcia, J.J. Fripiat, *Micropor. Mesopor. Mater.* 32 (1999) 175.
- [15] J.L. Blin, R. Flamant, B.L. Su, *Int. J. Inorg. Mater.* 3 (2001) 959.
- [16] Y.Y. Huang, T.J. Mccarthy, W.M.H. Sachtler, *Appl. Catal. A* 148 (1996) 135.
- [17] G. Larsen, E. Lotero, M. Nabity, L.M. Petkovic, D.S. Shobe, *J. Catal.* 164 (1996) 246.
- [18] E. Zhao, S.E. Hardcastle, G. Pacheco, A. Garcia, A.L. Blumenfeld, J.J. Fripiat, *Micropor. Mesopor. Mater.* 31 (1999) 9.
- [19] D.S. Sood, S.C. Sherman, A.V. Iretskii, J.C. Kenvin, D.A. Schiraldi, M.G. White, *J. Catal.* 199 (2001) 149.
- [20] R.D. Howells, J.D. Mc Cown, *Chem. Rev.* 77 (1977) 69.
- [21] A. Senning, *Chem. Rev.* 65 (1965) 385.
- [22] D.G. Russel, J.B. Senior, *Can. J. Chem.* 52 (1974) 2975.
- [23] J.W. Brockington, R.H. Bennett, US patent 3,970,721, 1976.
- [24] J.F. Joly, C. Marcilly, E. Benazzi, US patent 5,336,833, 1994.
- [25] S.I. Hommeltoft, Eur. patent 0,987,237A, 2000.
- [26] D.Q. Zhou, J.H. Yang, G.M. Dong, M.Y. Huang, Y.Y. Jiang, *J. Mol. Catal. A* 159 (2000) 85.
- [27] A.N. Parvulescu, B.C. Gagea, M. Alifanti, V. Parvulescu, V.I. Parvulescu, S. Nae, A. Razus, G. Poncelet, P. Grange, *J. Catal.* 202 (2001) 319.
- [28] K. Wilson, A. Renson, J.H. Clark, *Catal. Lett.* 61 (1999) 51.
- [29] K. Bauer, D. Garbe, H. Surburg, *Common Fragrances and Flavors Materials*, second ed., VCH, New York, 1990.
- [30] A. Walczak, J. Rzasca, S. Labus, *Pol. PL.* 170632, 1997.
- [31] J.I. Kroschwitz, M. Howe-Grant (Eds.), *Kirk–Othmer Encyclopedia of Chemical Technology*, 4th ed., Wiley, New York, 1995, p. 454.
- [32] S. Hitz, R. Prins, *J. Catal.* 168 (1997) 194.
- [33] M. Chamumi, D. Brunel, F. Fajula, P. Geneste, P. Moreau, J. Solof, *Zeolites* 14 (1994) 283.
- [34] A.O. Bianchi, M. Champanati, P.M. Torres, E.R. Castellon, A.J. Lopez, A. Vaccari, *Appl. Catal. A* 220 (2001) 105.
- [35] U. Ciesla, S. Schacht, G.D. Stucky, K.K. Unger, F. Schuth, *Angew. Chem. Int. Ed. Engl.* 35 (1996) 541.
- [36] N.C. Marziano, L.D. Ronchin, C. Tortato, A. Zingales, A.A. Sheikh-Osman, *J. Mol. Catal. A* 174 (2001) 265.
- [37] G. Herzberg, *Infrared and Raman Spectra of Polyatomic Molecules*, Van Nostrand, New York, 1945, p. 285.
- [38] L.J. Bellamy, *The Infrared Spectra of Complex Molecules*, Wiley, New York, 1960, p. 328.
- [39] C.J. Pouchert, *The Aldrich Library of IR Spectra*, 3rd ed., 1981, p. 533.
- [40] C.J. Pouchert, J. Behnke, *The Aldrich Library of ¹³C and ¹H FT NMR Spectra*, Vol. 1, p. 1431.
- [41] Y. Katsuhara, R.M. Hammaker, D.D. DesMarteau, *Inorg. Chem.* 19 (1980) 607.
- [42] H.G.M. Edwards, *Spectrochim. Acta* 45A (1989) 715.
- [43] T. Hall, P.K. Hansma, *Surf. Sci.* 71 (1978) 1, and references therein.
- [44] M. Chidambaram, C. Venkatesan, P.R. Rajamohanam, A.P. Singh, *Appl. Catal. A: Gen.* 244 (2003) 27.
- [45] C.H. Rochester, *Acidity Functions*, Academic Press, London, 1970.
- [46] G.A. Olah, G.K. Surya Prakash, J. Sommer, *Science* 206 (1973) 13.
- [47] A. Corma, M.I. Fornes, J.M. Juan-Rajadell, L. Neito, *Appl. Catal. A* 116 (1994) 151.
- [48] X. Ju, P. Huang, N. Xu, J. Shi, *J. Membr. Sci.* 166 (2000) 41.
- [49] S.C. Laha, P. Mukherjee, S.R. Sainkar, R. Kumar, *J. Catal.* 207 (2002) 213.
- [50] M.S. Wong, J.Y. Ying, *Chem. Mater.* 10 (1998) 2067.
- [51] D.M. Antonelli, *Adv. Mater.* 11 (1999) 487.
- [52] M.S. Wong, J.Y. Ying, *Chem. Mater.* 10 (1998) 2067.
- [53] J.A. Wang, M.A. Valenzuela, J. Salmones, A. Vazquez, A.G. Ruiz, X. Bokhimi, *Catal. Today* 68 (2001) 21.